

Geometrically frustrated GdInO_3 : An exotic system to study negative thermal expansion and spin-lattice coupling

Barnita Paul, Swastika Chatterjee and Anushree Roy*

Department of Physics, Indian Institute of Technology Kharagpur 721302, India.

A. Midya and P. Mandal†

Saha Institute of Nuclear Physics, 1/AF Bidhannagar, Calcutta 700 064, India.

Vinita Grover and A.K. Tyagi

Chemistry Division, Bhabha Atomic Research Centre, Mumbai 400085, India.

Abstract

In this article, we report negative thermal expansion and spin frustration in hexagonal GdInO_3 . Rietveld refinement of the XRD patterns reveal that the negative thermal expansion in the temperature range of 50-100K stems from the triangular lattice of Gd^{3+} ions. At low temperature, the downward deviation of the inverse susceptibility (χ^{-1}) vs. T plot from the Curie-Weiss law indicates spin frustration which inhibits long-range magnetic ordering down to 2K. Magnetostriction measurements clearly demonstrate a strong spin-lattice coupling. Low temperature anomalous phonon softening, as obtained from temperature dependent Raman measurements, also reveals the same. Our experimental observations are supported by first principles density functional theory calculations of the electronic and phonon dispersion of GdInO_3 . The calculations suggest that the GdInO_3 lattice is highly frustrated at low temperature. Further, the calculated normal mode frequencies of the Gd related Γ point phonons are found to depend on the magnetic structure of the lattice, suggesting significant magneto-elastic coupling.

*Electronic address: anushree@phy.iitkgp.ernet.in

†Electronic address: prabhat.mandal@saha.ac.in

I. INTRODUCTION

In recent years, ABO_3 -type (A=rare-earth, B=transition metal) rare-earth ferrites, manganites or nickelates find a special interest due to their multiferroic characteristics [1–6]. The role of d -shell electrons of B ions, governing the multiferroic properties of these systems, has been explored extensively. Unlike the above materials, if B belongs to a non-transition metal ion, the electric or magnetic properties of the system are expected to arise only from the $4f$ -shell electrons of the rare-earth ion, A. In this regard, rare earth indates, $REInO_3$, have emerged as potential candidates for fascinating ferroelectric memory devices [7–10]. The non-centrosymmetric atomic arrangement in the hexagonal unit cell of this system gives rise to the geometric ferroelectricity [11]. Among all compounds in the rare-earth indate series, $GdInO_3$ draws a special attention because of the presence of Gd^{3+} ion, which has exact half-filled $4f$ shell as the outermost orbital. Gd^{3+} ion shows pure spin magnetism with $\vec{L} = 0$, $\vec{J} = \vec{S} = 7/2$. Due to the isotropic g-factor, specifying the magnetic moment of Gd^{3+} , one expects $GdInO_3$ as a classical Heisenberg system. Furthermore, in the literature we find that some of the Gd based compounds exhibit the negative thermal expansion (NTE). While the mechanism of NTE in crystalline Gd [12] is associated with the change in magnetic ordering, the same is attributed to the transverse vibrational motion of two-coordinated Pd atom in $GdPd_3B_{0.25}C_{0.75}$ [13]. This indicates the origin of NTE to depend on the crystalline environment of Gd ions in a system. Along with large spontaneous polarization [11], the possibility of appearance of above discussed features marks $GdInO_3$ as an exotic system. Although In^{3+} does not play any direct role on spin ordering in $GdInO_3$, the non-centrosymmetric distortion in the crystal structure due to large In^{3+} ion is expected to yield a complex interplay between spin and lattice degrees of freedom in this system.

In the present work, we discuss the magnetic ordering, the crystal structure and the possibility of spin and lattice coupling in $GdInO_3$ compound. We have observed NTE in this system over the temperature range between 50K and 100K. The role of Gd^{3+} ions for NTE is evident from the Rietveld refinement of low temperature X-ray diffraction (XRD) patterns. In addition, the spin frustration in this system is confirmed from the temperature dependence of the magnetic susceptibility below 150K. Low temperature magnetostriction measurements indicate strong spin-phonon coupling in this system. The anomalous softening of the phonon mode in the low temperature range also reveals the same. Experimental observation has

been further supported by the first principles density functional theory (DFT) calculations of the electronic and phonon dispersion in GdInO_3 . Our calculations find that the lattice is highly frustrated and that there does exist a substantial amount of spin-lattice coupling in this system. The present article is organized as follows. In Section II, we have discussed the experimental and computational details. Section III presents the results regarding NTE and spin frustration in GdInO_3 . Following which the spin-lattice coupling in this system is discussed. Finally, in section IV we have summarized our results.

II. EXPERIMENTAL AND COMPUTATIONAL DETAILS

Bulk powder of GdInO_3 was prepared by self-assisted gel combustion method. Stoichiometric amount of Gd_2O_3 and In_2O_3 were dissolved in nitric acid followed by an addition of glycine. Glycine acts as both fuel and complexing agent. A gel was formed by evaporating the solution at the temperature of 80-100°C. It was then further heated up to 250°C. The obtained powder was calcined at 550°C for 1 h and then annealed at 850°C for 12 hrs. The details of the synthesis procedure are reported elsewhere [11].

Raman measurements on all samples were carried out using a micro-Raman spectrometer (TRIA550, JY, France), equipped with a Peltier-cooled charge coupled device (CCD) as the detector. A laser irradiation of 488 nm wavelength with 3 mW laser power was used as an excitation source to avoid the heating of the sample. A 50L× microscope objective was used for focusing the light on the sample. Temperature variation was carried out using a sample stage and a temperature controller along with a liquid nitrogen pump (THMS-600, Linkam, UK) over the temperature range 78K to 300K. From 300K to 240K, spectra were recorded at a temperature interval of 15K whereas at 10K interval over the range of 230–180K and 5K interval for 175K to 78K.

All magnetization measurements were carried out using SQUID VSM (Quantum Design). We have measured the sample length change in the temperature range 2–300 K of typical length ~ 1 mm by the capacitive method using a miniature tilted-plate dilatometer. The longitudinal magnetostriction was measured with field applied parallel to the sample length.

First principles calculations were performed within the framework of density functional theory (DFT) [14, 15] using the projector augmented wave (PAW)[16, 17] method as implemented in the plane-wave based VASP code [18–20]. The exchange-correlation functional

was chosen to be the Perdew-Burke-Ernzerhof (PBE) [21] implementation of the generalized gradient approximation (GGA). An energy cut-off of 450 eV was used for plane wave expansions. To include the strong correlation effects of $4f$ electrons of Gd, we used the spin-polarized GGA plus Hubbard U (GGA+U) [22] method, as in the Dudarev's implementation [23], with $U-J=4.6$ eV [24]. The ionic positions as well as the lattice parameters have been relaxed using conjugate-gradient algorithm, until the Hellmann-Feynman forces become less than 0.005 eV/Å. The energy convergence with respect to the computational parameters was carefully examined. The Γ point phonon frequencies have been calculated using the density functional perturbation theory (DFPT) [25] as implemented in the VASP code.

III. RESULTS AND DISCUSSION

A. Structural anomaly and spin-frustration in GdInO₃

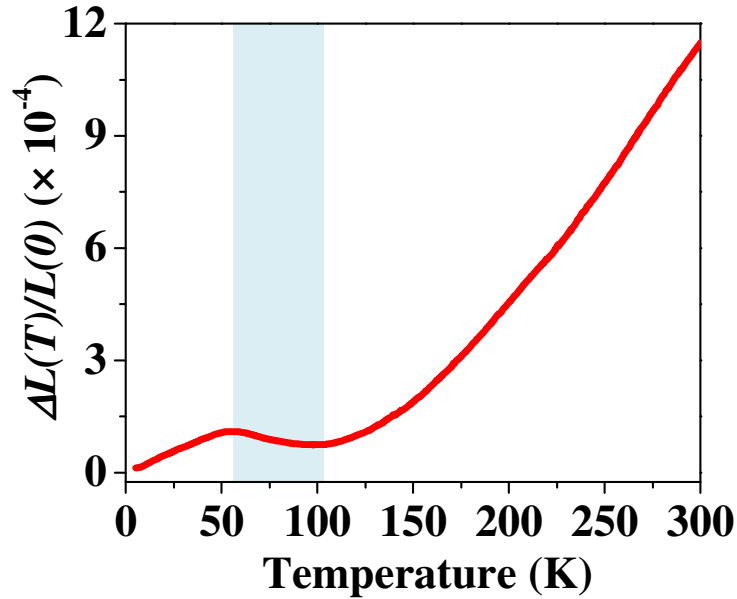


FIG. 1: Temperature dependence of the relative length change $\Delta L/L(0)$. Blue shaded zone marks the temperature range for negative thermal expansion.

Fig. 1 displays the coupling of temperature with lattice degrees of freedom in GdInO₃, by plotting the relative thermal expansion of the sample length, defined by $\frac{\Delta L}{L(0)} \equiv \frac{L(T)-L(0)}{L(0)}$,

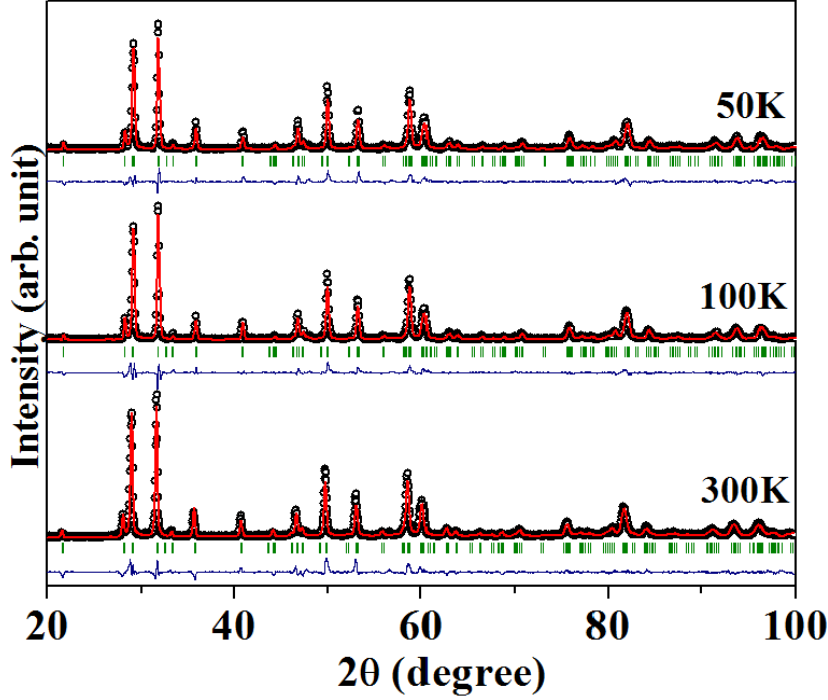


FIG. 2: Rietveld refined pattern of GdInO_3 at 50K, 100K and 300K. The red lines are the fitted patterns. The green bars show the positions of Bragg reflection peaks and the blue lines are the difference between the experimental and calculated patterns in each panel.

over the temperature range between 5K and 300K. $L(0)$ is the length of the sample at 5K (the lowest temperature at which the measurement was carried out). Below room temperature, the plot exhibits expected monotonic decreasing trend till 100K. Between 100K and 50K, the value of ΔL increases with decrease in temperature, followed by a smooth downturn upon further lowering of the temperature. The increase in ΔL with lowering of temperature, over the range between 50 K and 100K, indicates NTE of the system in this range of temperature.

To decipher the origin of NTE, as seen in Fig. 1, we probe the effect of temperature on the crystal structure of the GdInO_3 . Fig. 2 shows the powder XRD patterns of the compound at 50K, 100K and 300K. Rietveld refined patterns are shown by red solid lines in the figure. All patterns could be fitted with non-centrosymmetric $\text{P6}_3\text{cm}$ space group. This rules out the possibility of any structural phase transition to be the origin of NTE, observed in Fig. 1, in the temperature range between 50K and 100K. Fig. 3(a) plots the lattice parameters, a , c and unit cell volume (V) at three temperatures, as obtained from the Rietveld analysis of the diffraction data. It is to be noted from Fig. 1 that for GdInO_3 , the linear thermal

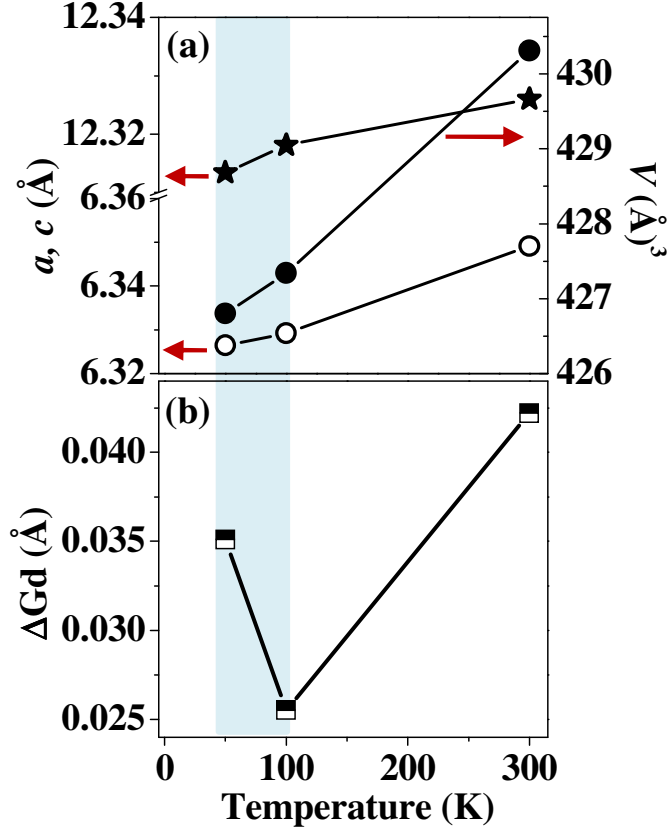


FIG. 3: (a) Variation in a (○), c (★), and cell volume (V ,●) and (b) ΔGd with temperature. The error bars are within the size of the symbols.

expansion coefficient α_L is of the order of 10^{-6} K^{-1} . Thus, it is non-trivial to find the reflection of the expected small change in the lattice parameters between 50K and 100K in the XRD patterns of the sample. Therefore, instead of analyzing the change in lattice parameters, we carefully examined bond distances between ions in the refined structure. It is to be noted that this may reveal the contribution of specific atomic plane in anomalous structural distortion for NTE.

The atomic arrangement of hexagonal GdInO_3 unit cell with non-centrosymmetric $P6_3cm$ space group is shown in Fig. 4(a). Gd1 and Gd2 are two inequivalent Gd atoms with Wyckoff positions 2a and 4b respectively. The hexagonal structure consists of tilted InO_5 bipyramids with two apical (O1, O2) and three planar oxygen ions (O3, O4, O4). Two inequivalent atomic positions of Gd ions form a triangular lattice, as shown in Fig. 4(b), between two InO_5 bipyramidal layers. Two different arm lengths, $d_1 = \text{Gd1-Gd2}$ (black dashed lines) and $d_2 = \text{Gd2-Gd2}$ (red dashed lines), are involved in forming the triangular lattice. Interestingly,

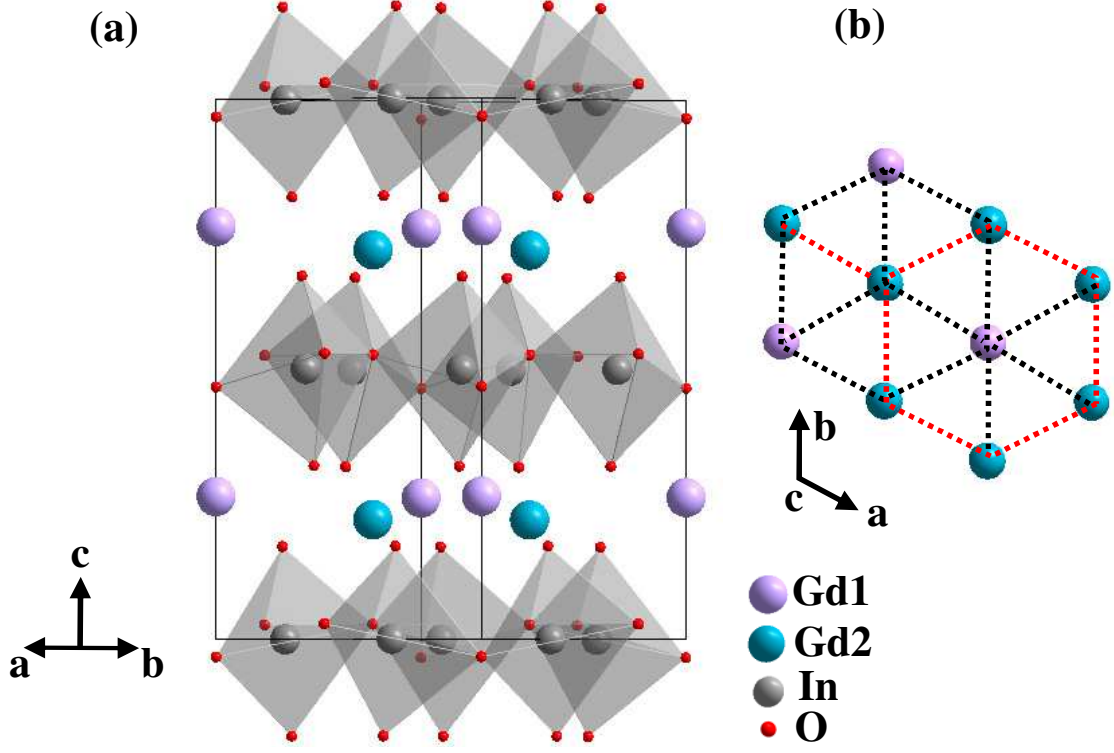


FIG. 4: (a) Crystal structure of hexagonal GdInO₃ and (b) triangular arrangement of Gd ions viewed along c-axis.

we find that the difference between these two distances, ($\Delta\text{Gd}=d_1 - d_2$), does not change monotonically with temperature, as shown in Fig. 3(b). At 300 K the difference is 0.0422 Å, which is 0.0255 Å at 100 K. The difference again increases to 0.0351 Å at 50K. Comparing Fig. 1(a) and Fig. 3(b) it appears that the above anomalous lattice distortion in the Gd plane is reflected in NTE of GdInO₃ over the temperature range between 50K and 100K.

To explore the magnetic behavior, we have carried out magnetization measurements at constant temperature ($M - H$ plot at 2K) and at constant field ($M - T$ plot at 50 Oe), Fig. 5 (a) and (b), respectively. The absence of hysteresis loop in $M - H$ plot suggests an absence of long range magnetic ordering in the system even down to 2K. However, the presence of short range magnetically ordered phase was identified from the temperature dependence of inverse susceptibility χ^{-1} ($=H/M$) plot, shown by the solid line in Fig. 5(b). Though the susceptibility follows the Curie-Weiss like behavior at high temperature, it shows a deviation from the linearity below 150K (the dashed line marks the expected Curie-Weiss linear plot), indicating a strong spin fluctuation in the paramagnetic phase of the system.

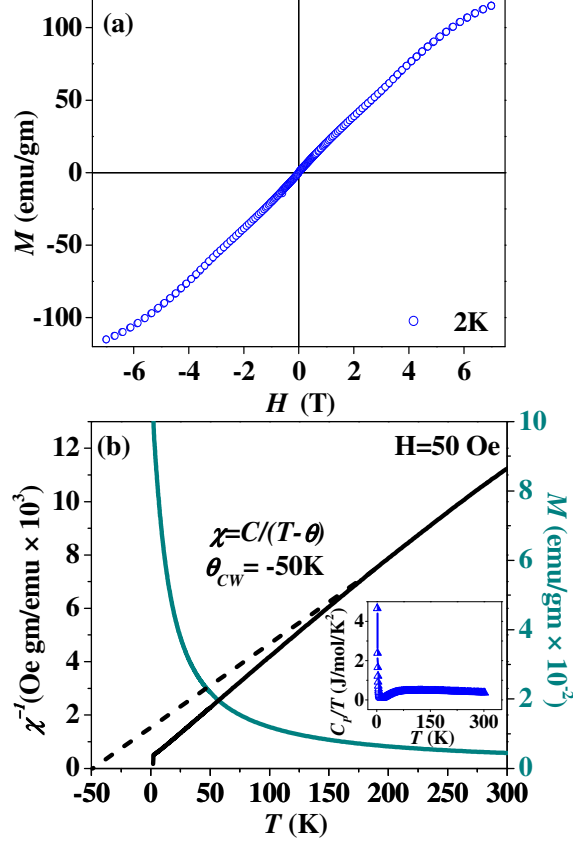


FIG. 5: (a) M-H curve at 2K, (b) Plot of M and χ^{-1} vs T (solid line). The dashed line corresponds to the Curie-Weiss law.

The extrapolated Curie-Weiss temperature (θ_{CW}) is found to be -50 K. The inset of Fig. 5 (b) plots the variation of specific heat with temperature (C_p/T vs. T). We observe a sharp upturn of the plot just below 1.8 K (Neel temperature, T_N). It is to be noted that χ^{-1} shows a sharp drop just below 1.8 K. Both of these observations suggest that antiferromagnetic (AFM) ordering takes place only below 1.8 K. The ratio of θ_{CW} and T_N (θ_{CW}/T_N), which estimates the degree of frustration, is found to be sufficiently large ~ 28 .

B. Spin-lattice coupling in GdInO_3

In above discussion we confirm the presence of short range magnetic ordering in GdInO_3 over a wide range of temperature. The antiferromagnetic ordering in the system is expected only below $T_N = 1.8$ K. Magnetostriction measurement is often used to study the strength of coupling between spin and lattice. $\Delta L(H)/L(0)$ i.e. $[L(H) - L(0)]/L(0)$ plots, recorded at

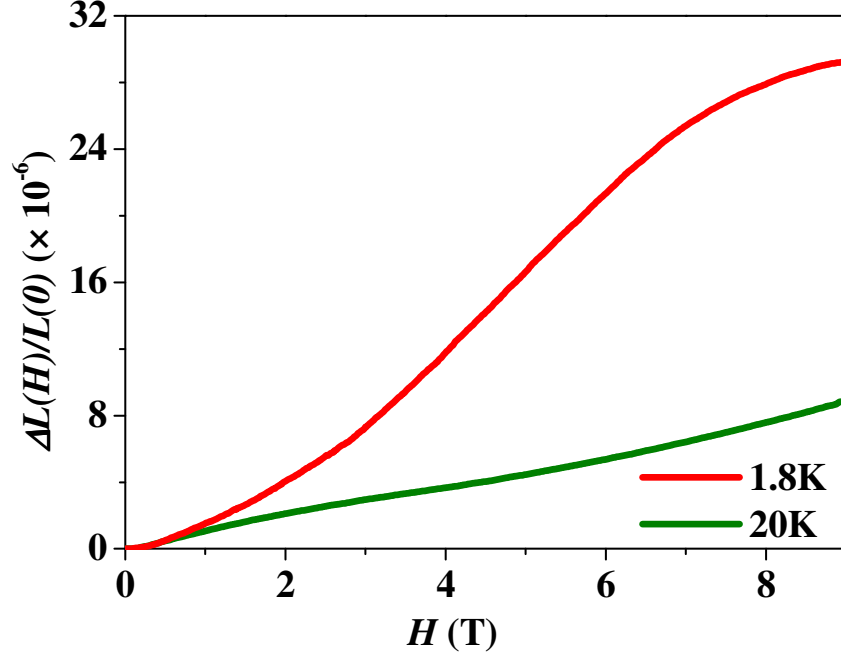


FIG. 6: Magnetostriction plotted as $\Delta L(H)/L(0)$ vs H at 1.8K and 20K.

1.8K and 20K are shown in Fig. 6. We find that at 1.8K, $\Delta L(H)/L(0)$ varies with applied magnetic field along with a change in slope at ~ 3 T. However, a very small change was observed for the same, recorded at 20K. It is to be noted that without any coupling between spin and lattice, we expect the $\Delta L(H)/L(0)$ plot to be independent of temperature. Above result is a clear indication of low temperature coupling of lattice and spin degrees of freedom in GdInO_3 .

Furthermore, the possibility of the coupling between the spin and lattice degrees of freedom has been probed by temperature dependent Raman measurements over the range between 78K and 300K, and shown in Fig. 7. All spectra were recorded over the spectral range of 200–700 cm^{-1} . The deconvolution of Raman spectra (after a linear background subtraction) by seven Lorentzian profiles provides us the evolution of Raman shift for all modes over the given range of temperature. We consider only the prominent Raman modes around $\sim 239 \text{ cm}^{-1}$, 321 cm^{-1} , 360 cm^{-1} , 373 cm^{-1} , 413 cm^{-1} and 607 cm^{-1} for further discussion. The atomic vibration corresponding to these modes have been discussed in details in our earlier report [11]. Fig. 8 plots the variation of the peak positions for the above mentioned modes (shown by symbols) with temperature, as obtained from the deconvolu-

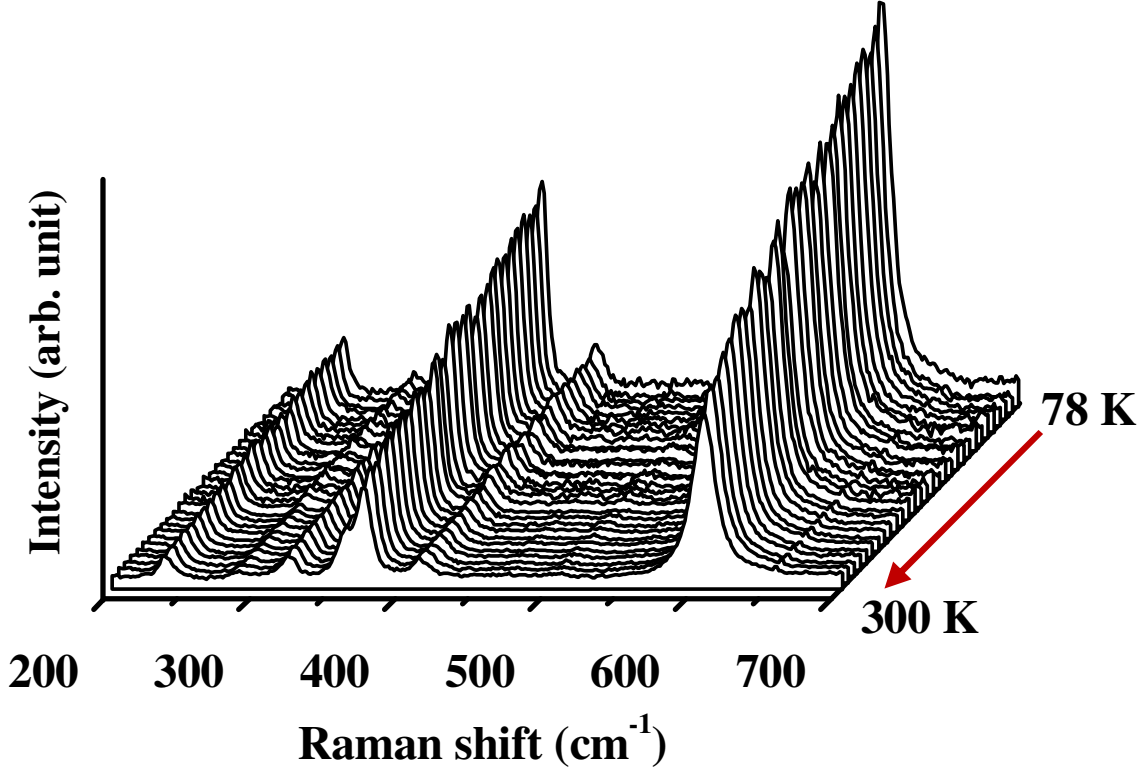


FIG. 7: Temperature dependent Raman spectra of GdInO_3 in the spectral range of 200 to 700 cm^{-1} after linear baseline correction.

tion of the spectra. The corresponding atomic vibrations of all Raman modes from Ref. [11] are mentioned in each panel of Fig. 8. The change in Raman shift with temperature at a constant pressure can be expressed as follows [26, 27],

$$\left(\frac{d\omega}{dT}\right)_P = \left(\frac{\partial\omega}{\partial T}\right)_V + \left(\frac{\partial\omega}{\partial V}\right)_T \left(\frac{\partial V}{\partial T}\right)_P. \quad (1)$$

Using the following definitions of Grüneisen parameter (γ) and volume thermal expansion coefficient (α_V),

$$\gamma = -\frac{\partial(\ln\omega)}{\partial(\ln V)}; \alpha_V = \frac{1}{V} \left(\frac{\partial V}{\partial T}\right), \quad (2)$$

Eqn.1 becomes

$$\frac{1}{\omega} \left(\frac{d\omega}{dT}\right)_P = \frac{1}{\omega} \left(\frac{\partial\omega}{\partial T}\right)_V - \gamma\alpha_V. \quad (3)$$

The first term in R.H.S of Eqn. 3 represents the true anharmonic contribution of the temperature on the mode frequency due to the anharmonic potential. The second term represents the change in the frequency due to the change in cell volume with temperature.

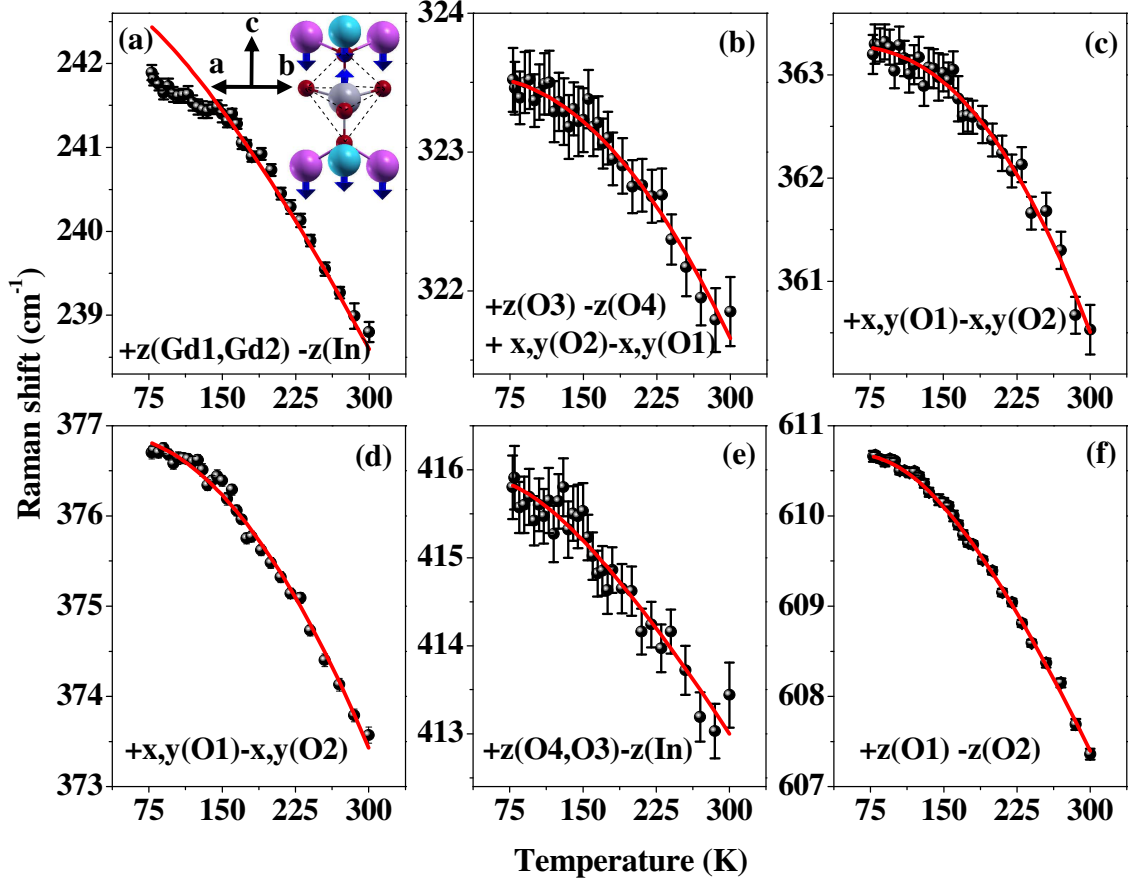


FIG. 8: Evolution of Raman modes (mentioned in the text) with temperature for GdInO_3 . The inset of panel (a) schematically shows the atomic displacement patterns of the corresponding phonon mode as mentioned in ref [11] involving Gd1(magenta spheres), Gd2(cyan spheres), In(grey spheres) and O(red spheres). The blue arrows mark the directions of the vibration of the atoms involved.

In our case, the thermal expansion coefficient $\alpha_V \approx 3\alpha_L$ is only $\sim 10^{-6}$ (refer to Fig. 1), and hence the contribution of volume contraction on the change in the frequency of the phonon modes with lowering of temperature can be neglected. Thus, in Fig. 8 we analyze the experimentally obtained data points only by considering the true anharmonic contribution of temperature on the phonon frequency. The solid red lines are generated by taking into account the four phonon decay process due to the increase in anharmonicity in the vibrational potential with temperature [28] by following the relations

$$\omega_{anh} = \omega_0 + \Delta(T),$$

$$\Delta(T) = A \left(1 + \frac{2}{(e^{\phi/2} - 1)} \right) + B \left(1 + \frac{3}{(e^{\phi/3} - 1)} + \frac{3}{(e^{\phi/3} - 1)^2} \right), \quad (4)$$

where, ω_0 is the phonon frequency at 0K, $\phi = \hbar\omega_0/k_B T$ and A and B are anharmonic constants.

We find that data points for all modes, except the one at 239 cm^{-1} could be fitted by a set of constants A , B and ω_0 for each, for the whole range of temperature between 78K and 300K (see the red solid lines in panel (b) to (f) in Fig. 8). The clear change in the slope of observed phonon frequency of the Raman mode at 239 cm^{-1} near 150K compelled us to fit the data points with free fitting parameters up to 150K using Eqn. (1) and (2) [refer to the red solid line in the panel (a) of Fig. 8]. The deviation of the measured frequency of the Raman mode near 239 cm^{-1} from the expected anharmonic frequency (solid line) indicates an additional factor to be responsible for the anomalous shift. The atomic vibrations related to the Raman mode at 239 cm^{-1} involve vibration of Gd and In ions along the c axis, and is shown in the inset of panel (a) in Fig. 8. It is to be noted that this is the only mode, under study, which involves the vibration of Gd ions. The absence of such anomaly in other Raman modes (panel (b) to (f) in Fig. 8), confirms the role of magnetic Gd plane as the origin of the anomalous phonon softening and indicates the magneto-elastic coupling in this system. Here we would like to mention that the plot $\Delta L(H)/L(0)$ vs. H at 20K, as observed in Fig. 6, has much lesser slope than that at 1.8K. From this figure it appears that the spin-lattice coupling is much weaker at 20K. This, in a way, contradicts the Raman results, which exhibit the presence of spin-phonon coupling even at 150K. This can be justified by the fact that the magnetostriction measurement yields an average effect over all directions. In contrary, the mode we probe by Raman measurement involves the vibration of Gd^{3+} ion in specific direction as shown in the inset of Fig. 8(a).

The interplay between the spin and lattice degrees of freedom in GdInO_3 was further investigated using first principles calculations. The GdInO_3 lattice was fully optimized, starting from the room temperature experimental data. In order to determine the preferred magnetic orientation of Gd, we performed total energy calculations of all possible magnetic configurations of Gd in GdInO_3 lattice, as shown in Fig. 9. We find that all antiferromagnetic configurations are energetically very close, the difference being of the order of 0.001 eV ($\sim 10\text{K}$) and that they are higher than the ferromagnetic configuration by 0.01 eV. This clearly suggests that at 0K the GdInO_3 lattice is highly frustrated. An evidence of frustration

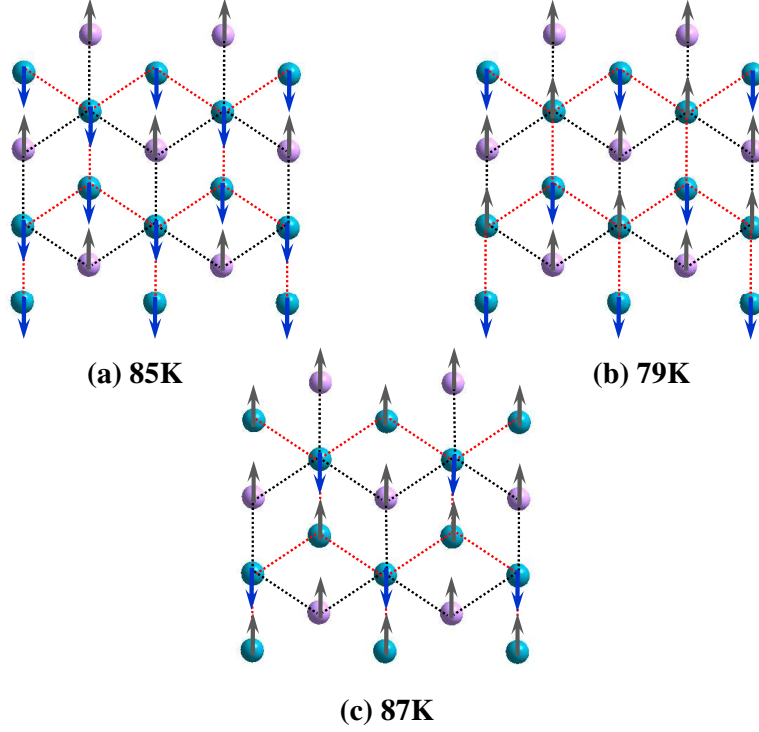


FIG. 9: Schematic diagram of all AFM configurations in Gd triangular lattice. The relative stabilization energy of different AFM configurations with respect to the FM configuration has been indicated at the bottom of each AFM configuration.

is also obtained, where we observe a decrease in the ΔG_d upon lowering of temperature. The estimated value of ΔG_d is 0.04 \AA at 300K and only 0.02 \AA at 0K. The change is very small. Nonetheless, there have been reports on change in magnetic ordering temperature upto 30K with only 0.1% change in lattice parameter [29].

We also studied the change in the phonon frequencies with change in the magnetic ordering of the Gd ions in GdInO_3 . For this purpose we calculated the Γ -point phonon spectra for ferromagnetic ordering of Gd ions and one of the many possible AFM alignments of the Gd ions in Fig. 9. An examination of the phonon modes indeed shows a softening as we alter the magnetic structure of the lattice as shown in Fig. 10. The calculated phonon mode near 230 cm^{-1} (the one which experimentally appeared at 239 cm^{-1}), which involves Gd ions is found to soften as we go from FM to AFM configuration. It is to be noted that without spin-phonon coupling, the phonon mode frequencies would not have been modified with a change in magnetic ordering of the system.

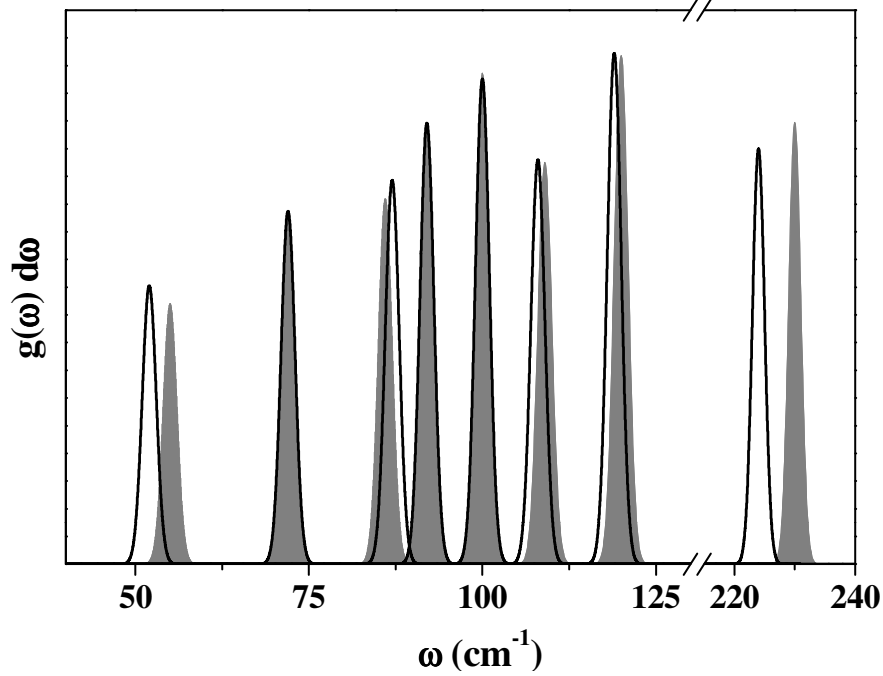


FIG. 10: Calculated phonon spectra of GdInO_3 for FM (shown by the filled area) and AFM (shown by the solid line) configuration at 0K.

IV. CONCLUSION

To summarize, we demonstrate NTE in hexagonal GdInO_3 at the temperature range of 50–100K. The corresponding change in the crystal structure is manifested in the triangular lattice of Gd^{3+} ions. The onset of spin frustration at 150K with a large frustration parameter hinders the long range magnetic ordering in the system and we find an antiferromagnetic ordering only at a very low temperature. Magnetostriction measurement and the anomalous softening of phonon mode of Gd-related atomic vibration indicate a spin-phonon coupling in this system. Our claims are further supported by first principle phonon calculations.

Acknowledgements Authors thank Dr. P.S.Sastry, BARC, Mumbai, for low temperature XRD measurements. AR thanks DST and BRNS, India, for financial assistance. SC thanks DST, India for the Inspire fellowship.

-
- [1] Z. J. Huang, Y. Cao, Y. Y. Sun, Y. Y. Xue, and C. W. Chu, Phys. Rev. B **56**, 2623 (1997).
 - [2] G. Giovannetti, S. Kumar, D. Khomskii, S. Picozzi, and J. van den Brink, Phys. Rev. Lett.

- 103**, 156401 (2009).
- [3] W. Wang, J. Zhao, W. Wang, Z. Gai, N. Balke, M. Chi, H. N. Lee, W. Tian, L. Zhu, X. Cheng, D. J. Keavney, J. Yi, T. Z. Ward, P. C. Snijders, H. M. Christen, W. Wu, J. Shen, and X. Xu, Phys. Rev. Lett. **110**, 237601 (2013).
 - [4] H. Das, A. L. Wysocki, Y. Geng, W. Wu, and C. J. Fennie, Nat. Commun. **5**, 1 (2014).
 - [5] C. Xu, Y. Yang, S. Wang, W. Duan, B. Gu, and L. Bellaiche, Phys. Rev. B **89**, 205122, (2014).
 - [6] A. Paul, P. Sharma, and U. V. Waghmare, Phys. Rev. B **92**, 054106 (2015).
 - [7] S. C. Abrahams, Acta Crystallogr., Sect. B: Struct. Sci. **57**, 485 (2001).
 - [8] T. Tohei, H. Moriwake, H. Murata, A. Kuwabara, R. Hashimoto, T. Yamamoto, and I. Tanaka, Phys. Rev. B **79**, 144125 (2009).
 - [9] R. Shukla, V. Grover, S. K. Deshpande, D. Jain, and A. K. Tyagi, Inorg. Chem. **52**, 13179 (2013).
 - [10] R. Shukla, F. N. Sayed, V. Grover, S. K. Deshpande, A. Guleria, and A. K. Tyagi, Inorg. Chem. **53**, 10101 (2014).
 - [11] B. Paul, S. Chatterjee, S. Gop, A. Roy, V. Grover, R. Shukla, and A. K. Tyagi, Mater. Res. Exp. (2016).
 - [12] Y. V. Ergin, Soviet Physics JETP **21**, 709 (1965).
 - [13] A. Pandey, C. Mazumder, R. Ranganathan, S. Tripathi, D. Pandey, and S. Dattagupta, Appl. Phys. Lett **92**, 261913 (2008).
 - [14] P. Hohenberg and W. Kohn, Phys. Rev. **136**, B864 (1964).
 - [15] W. Kohn and L. J. Sham, *ibid.* **140**, A1133 (1965).
 - [16] P. E. Blöchl, Phys. Rev. B **50**, 17953 (1994).
 - [17] G. Kresse and D. Joubert, Phys. Rev. B **59**, 1758 (1999).
 - [18] G. Kresse and J. Hafner, Phys. Rev. B **47**, 558 (1993).
 - [19] G. Kresse and J. Furthmüller, Comput. Mater. Sci. **6**, 15 (1996).
 - [20] G. Kresse and J. Furthmüller, Phys. Rev. B **54**, 11169 (1996).
 - [21] J. P. Perdew, K. Burke, and M. Ernzerhof, Phys. Rev. Lett. **77**, 3865 (1996).
 - [22] J. Hubbard, Proc. R. Soc. London Ser. A **276**, 238 (1963).
 - [23] S. L. Dudarev, G. A. Botton, S. Y. Savrasov, C. J. Humphreys, and A. P. Sutton, Phys. Rev. B **57**, 1505 (1998).
 - [24] M. Topsakal and R.M. Wentzcovitch, Computational Materials Science **95**, 263 (2014).

- [25] S. Baroni, S. de Gironcoli, A. Dal Corso, and P. Giannozzi, *Rev. Mod. Phys.* **73**, 515 (2001)
- [26] P. S. Peercy and B. Morosin, *Phys. Rev. B* **7**, 2779 (1973).
- [27] T. R. Ravindran, A. K. Arora, and T. A. Mary, *Phys. Rev. B* **67**, 064301 (2003).
- [28] M. Balkanski, R. F. Wallis, and E. Haro, *Phys. Rev. B* **28**, 1928 (1983).
- [29] A. K. Singh, S. Patnaik, S. D. Kaushik and V. Siruguri, *Phys. Rev. B* **81**, 184406 (2010).